RSC Advances

This is an *Accepted Manuscript*, which has been through the Royal Society of Chemistry peer review process and has been accepted for publication.

Accepted Manuscripts are published online shortly after acceptance, before technical editing, formatting and proof reading. Using this free service, authors can make their results available to the community, in citable form, before we publish the edited article. This *Accepted Manuscript* will be replaced by the edited, formatted and paginated article as soon as this is available.

You can find more information about *Accepted Manuscripts* in the Information for Authors.

Please note that technical editing may introduce minor changes to the text and/or graphics, which may alter content. The journal's standard Terms & Conditions and the Ethical guidelines still apply. In no event shall the Royal Society of Chemistry be held responsible for any errors or omissions in this *Accepted Manuscript* or any consequences arising from the use of any information it contains.

ROYAL SOCIETY OF CHEMISTRY

www.rsc.org/advances

Low-temperature facile solution-processed gate dielectric for combustion derived oxide thin film transistors

Han Wang[1], Tieyu Sun[2], Wangying Xu[1], Fangyan Xie[3], Lei Ye[1], Yubin Xiao[1], Yu Wang[2], Jian Chen[3], Jianbin Xu[1]*

[1]Department of Electronic Engineering and Materials Science and Technology Research Center, The Chinese University of Hong Kong, Shatin, N.T., Hong Kong SAR, P. R. China

[2]Department of Applied Physics and Material Research Center, The Hong Kong Polytechnic University, Kowloon, Hong Kong SAR, P. R. China

[3]Instrumental Analysis & Research Center, Sun Yat-Sen (Zhongshan) University, Guangzhou, P. R. China

jbxu@ee.cuhk.edu.hk

Abstract

In this work, acetylacetone assisted solution-processed In-Ga-Zn-O (IGZO) thin film transistors (TFTs) using Al_2O_3 as gate dielectrics were investigated. Normally fully covered Al_2O_3 thin films are difficult to achieve by spin coating with conventional solvent, such as 2-methoxyethanol, due to the poor wettability of highly doped silicon. Here a conventional aluminum nitrate solution with an additive was designed, to spin coat robust continuous Al_2O_3 thin films, resulting from improved solution hydrophilic with a contact angle of 17°. For active layer fabrication, we utilized the previous reported combustion process to lower treatment temperature, which could be confined in the range from 220 °C to 300 °C, without losing the device performance. Results show that all the devices performed well. Especially, after 240 °C annealing of both Al_2O_3 (in thickness of around 45 nm) and IGZO thin films (in thickness of about 30 nm), we have obtained the following device parameters, namely a Al_2O_3 dielectric

RSC Advances Accepted Manuscript

breakdown electric field at 7.8 MV/cm, a current density around 1×10^{-6} A/cm^2 in the voltage range of −3 V to 3 V, a areal capacitance of 291 nF/cm^2 at 100 Hz, a carrier mobility of 0.74 cm^{2}V^{-1}s^{-1}, a threshold voltage of −0.4 V, a current on-off ratio of 6×10^3, a subthreshold swing of 375 mV/decade. Fabrication of combustion-processed active layers and our facile solution processed high-k dielectrics provides a feasible approach for low cost oxide flexible TFTs applications.

Keywords: solution process; Al_2O_3 dielectrics; frequency dispersion; combustion; IGZO TFTs; low temperature;

1. Introduction

Oxide based semiconductor devices, especially thin film transistors (TFTs), have been studied for decades as they are essentially important building blocks in optoelectronic devices.[1, 2] Until now oxide materials are widely explored because of their earth abundance, low cost, environmental friendly and easy processing, which are favorable for industry production and sustainable development. [3, 4] To replace traditional silicon dioxide dielectrics, much smaller working voltage with an augmented TFTs mobility were anticipated from some oxide TFTs gate dielectric candidates such as Al_2O_3, ZrO_2, TiO_2, et al , due to proper trade-off among dielectric constant, energy gap and conduction band offset on silicon. [5-11] On the other hand, ZnO based semiconductors, such as In-Zn-O (IZO), Zn-Sn-O (ZTO), IGZO are superior candidates towards TFTs active channel, featured by amorphous phase but excellent field effect performance under a relative low processing temperature in comparison with crystalline active-layer TFT.[12-15] As a result, zinc oxide based TFTs have received an extensive attention on lowering processing temperature, so as to ensure their various potential applications.[16-18]

Recently, solution-processed approach turns to be a major fabrication route for TFT active channels due to its advantages such as easy operation, vacuum free, controllable element stoichiometric ratio.[19-22] However, in comparison with conventional physical deposition processes, namely radio frequency magnetron sputtering, solution-

RSC Advances Accepted Manuscript

processed technique still require a high annealing temperature to facilitate precursor transform to oxide and at the same time to dense the film. Therefore to address that problem, a combustion route has been developed by lowering the annealing temperature successfully by Tobin Mark's group. [23-26] The key point is to introduce either urea or acetylacetone to serve as fuel. As soon as a moderate temperature is provided to drive the reaction, coordinating with oxidizer of NO^{3-}, the fuel then gives rise to a high enthalpy change in the exothermic reaction, soon afterwards forming a self-energy-generation system to continue a thorough chemical reaction.

Gate dielectric also plays a significant role on TFT performance. To ensure a low leakage current density and high breakdown voltage, the frequently used fabrication route is physical deposition. For example, pulsed laser deposition and radio frequency magnetron sputtering.[27, 28] In addition, with regard to solution process, a thorny challenge on poor wettability of highly doped silicon and inferior hydrophilic of general solvent also need to be settled. 2-methoxyethanol is one of the general solvent in spin-coating process on thermal grown SiO_2 substrates but its spin window is quite narrow on highly doped silicon substrates, which implies that a high quality film is hardly obtained even after an effective oxygen plasma or piranha solution treatment to obtain a super hydrophilic surface on substrates by attaching hydroxyl groups.[8, 10]

In this report, aiming to fabricate high performance oxide TFTs via a low processing temperature and facile procedures, a bunch of all solution processed TFTs have been systematically investigated. Firstly Al_2O_3 thin film, a high-k oxide dielectric, was successfully fabricated by an additive-assisted solution process. By utilizing acetylacetone and aqueous ammonia as an additive in 2-methoxyethanol, $Al(NO_3)_3$ solution can be spin-coated and fully covered onto substrates easily. This indicates the novel solution system broadens the fabrication window tremendously. In combination with combustion processed IGZO active layers, we demonstrated that by utilizing novel chemical processed Al_2O_3 as dielectric, after a mere 240°C annealing on both gate dielectric and active channel, TFT devices showed a mobility of 0.74 $cm^2V^{-1}s^{-1}$, an operating voltage range and threshold voltage in −3V to 3V, and −0.4V, respectively.

RSC Advances Accepted Manuscript

Beyond that, when processing temperature increased to 260 ºC, a mobility was increased to 2.26 $cm^2V^{-1}s^{-1}$, a threshold voltage was reduced to 0 V. The trade-off between treatment temperature and field effect performance implies a feasible trail of low cost and easy processing of flexible devices fabrication. Although acetylacetone is utilized in both dielectric and semiconductor layer fabrication, the role is totally different, which means it serves as an additive in Al^{3+} solution to improve wettability (after spin coating, acetylacetone volatilizes out at 120ºC.) while serving as a fuel in IGZO solution to participate in the reaction at no less than 220ºC.

2. Results and Discussion

To demonstrate the improved wettability of the novel Al_2O_3 precursor solution, we compared the contact angles of three solutions dropping onto highly doped silicon substrates without oxygen plasma treatment: conventional solution without additive; conventional solution with acetylacetone only and our novel solution. The measurements were shown in figure 1. The contact angles were 26º, 24º and 17º, respectively. It seems that the difference is small and could be ignored, but after the solution is dropped onto oxygen plasma treated highly doped silicon substrates, just aging without any further action, the wettability varies. (The contact angles are failed to be measured through contact angle microscope due to the super hydrophilic resulting from oxygen plasma treatment.) Then we pictured the spreadability of these three solution, after a drop of solution from syringe is added on the oxygen plasma treated highly doped silicon substrates and aging for 5 min, as shown in figure 2, to demonstrate the wettability of three solutions. After the additive of acetylacetone and aqueous ammonia is introduced in, solution wettability is improved significantly. The reason is the carbonyl group of acetylacetone and amido group of aqueous ammonia are both hydrophilic, hence they are benefit for solution wettability. In addition, the conventional solution of additive of aqueous ammonia only cannot be obtained because of the product of unsolvable $Al(OH)_3$ coming from the reaction. Among the media of acetylacetone, it obstructs the reaction between Al^{3+} and aqueous ammonia so that

RSC Advances Accepted Manuscript

aqueous ammonia can be added successfully with a concentration of no more than 60% of acetylacetone's. To further approve the facility of the novel solution, a comparison of thin film quality after spin coating and annealing between conventional and novel solution was also conducted. Figures 3(a) (b) and (c) showed optical microscope pictures of the samples, all of which were 2 layers, all of the final annealed temperatures were 220 ℃. Without any additives, spin-coated thin film is partial covered on substrates and seems uneven. The blue parts are of 2 layers, the brown parts are of 1 layer, and the white round shaped part is uncovered substrate. With an additive of acetylacetone and aqueous ammonia, when conducting a combustion process, which means annealing the thin film at 220ºC directly, poor quality films forms with a big mass of pores (the white random-shaped dots); while conducting a step annealing starting from 120ºC, to avoid combustion process, the spin-coated thin film (the brown part) has been fully covered on substrates, and seems very uniform. The white round one are Al electrodes with a radius of 100 μm. A superior wettability of solution guarantees a good quality of thin films.

As far as novel chemically-processed Al_2O_3 gate dielectrics, x-ray diffraction characterization of Al_2O_3 obtained after annealing at 300 ºC is shown in figure 4. Since no obvious diffraction peaks were observed, the fabricated Al_2O_3 dielectrics were amorphous, in favor of minimizing leakage current, and maximizing breakdown voltage, attributed to the absence of crystal grain boundaries. Surface morphologies of the Al_2O_3 film surfaces obtained after annealing at 220 ºC and 300 ºC were examined by AFM under tapping mode, as shown in figures 5(a), (b). Scan scale was 1 μm × 1 μm. It reveals that after spin-coated twice through a 0.3 M $Al(NO_3)_3$ solution, the surfaces were not as extremely smooth as thermal SiO_2 surface (RMS ~0.19 nm), but reached a RMS roughness of 0.5 nm and 1.1 nm, respectively. The roughness mainly came from the film growth and densification processes. Because of nucleation and coalescence of chemical species, the film growth resulted in a noticeable ups and down on the substrate plane, while the densification process resulted in formation of mesoscopic holes.

RSC Advances Accepted Manuscript

x-ray photoemission spectroscopy analysis of Al_2O_3 films obtained after annealing was performed to interrogate chemical states of oxygen, shown in figure 6(a). After deconvolution of the O 1*s* peak of Al_2O_3 thin films, three peaks centered at 532.0 eV, 532.8 eV and 534.0 eV can be told separately. The peak centered at 532.0 eV can be assigned to lattice oxygen which forms fully bonds with aluminum atoms. The peak centered at 532.8 eV can be assigned to the oxygen atoms which are not fully bound within the oxide, which usually related to the oxygen vacancy in oxygen-deficient regions. As the partial bonds with its surroundings, the peak towards to a higher binding energy than fully bound oxygen. The peak centered at 534.0 eV can be assigned to oxygen in hydroxide. Since hydrogen is more electronegative than the metals, the M-OH oxygen atoms are less negatively charged than those in oxides, shifting the XPS feature toward a much higher binding energy. [12, 15, 20] The relative fractions of these three species were calculated from the XPS semi-quantitative analyses. The relation between the percentages of oxygen species and the annealing temperature are shown in figure 6(b). As increase of annealing temperature, the change of concentration on oxygen vacancy is unobvious, meanwhile the concentration of oxygen in hydroxide decreases and lattice oxygen increases. The results suggest a higher annealing temperature is in favor of decomposing $Al(OH)_3$ to Al_2O_3.

Dielectric characteristics were measured through the (metal-insulator-metal) MIM structure of Al_2O_3 thin film. Current density versus breakdown electric field characteristic was shown in figure 7(a). Breakdown electric field of all samples were all no lower than 6.5 MV/cm. Due to the increase of oxygen vacancy as annealing temperature raised, the breakdown electric field degraded. However, after spin coating twice and film thickness increasing to around 45 nm, a greatly increased breakdown electric field is achieved. Thus even as low as an annealing temperature of 300 ^{o}C, the breakdown electric field was still closed to 7.5 MV/cm, laying a good foundation for TFT applications. The current density versus voltage of Al_2O_3 dielectrics was shown in figure 7(b). In order to match TFTs operating voltage range in convenience, here we adopt voltage instead of electric field as abscissa. The results indicated that leakage

RSC Advances Accepted Manuscript

current density were approximately to 10^{-6} A/cm^2 in the operating voltage range of −3 V to 3 V (Gate voltage of fabricated TFT was −3 V to 3 V), regardless of annealing temperature. The performed leakage current is acceptable in TFTs applications. Relationship between areal capacitance of Al_2O_3 films and frequency obtained by capacitance-voltage measurement in both ambience and vacuum were shown in figures 8(a) and (b). The capacitance density rises with increasing annealing temperature, because of the increase of Al_2O_3 percentage. The results also demonstrate an obvious frequency dispersion in low frequency range, which indicates the increase of capacitance density with decreasing frequency, like reference [10, 29] Comparing with capacitance in ambient and vacuum environments, it is obvious that the frequency dispersion and capacitance in vacuum are quite smaller than those in ambience, which may suggests an existence of proton conduction in ambient condition. [30-33] The proton mobile ion from absorbed water in ambience induces a great capacitance, through its migration and formation of an electric double layer (EDL) under a voltage bias. When the gate electrode is positive biased, proton migrates to the interface of dielectric and semiconductor, composing of a Helmholtz layer. However, because of the slow migration rate, the induced capacitance only responses in low frequency range, bringing obvious frequency dispersion. Characterization of phase angle and conductivity versus frequency in ambient environment are shown in figures 9(a) and (b). It is known that the phase angle of an ideal capacitor is -90° while it is 0° for an ideal resistor. [30, 31] The fabricated Al_2O_3 dielectrics perform as a capacitor in all frequency range. This result suggests the polarization within the dielectric media dominates the capacitance and frequency dispersion. The conductivity is also frequency-dependent. Similar phenomenon is also found in others work.[34] This is due to the ionic migration in ion-conducting disordered solid materials, causing the leakage current.[34]

Besides the proton conduction, here we also understand the frequency dispersion phenomenon through the fundamental of intrinsic dielectric, as the Al_2O_3 dielectrics perform a capacitor behavior all through the frequency range. Dielectric constants comes from dipole moment, in other words, coming from polarization of dielectrics.

RSC Advances Accepted Manuscript

There are basically three kinds of polarizations in the system: (1) electronic polarization which comes from Al_2O_3, (2) space charge polarization which comes from trapped charges which is related to oxygen vacancies and mobile charges which is related to hopping from hydroxyl sites, (3) orientation polarization which also comes from hydroxyl groups. Electronic polarization, which due to elastic displacement of electron clouds requires a very short time to perform, so it is almost frequency independent. Space charge and orientation polarization both come from the movements of charged particles, such as orientation of dipoles and migration of electrons, hence they require a longer time to perform, so they are major frequency dependent. Within low frequency range, electronic polarization has enough time to response to external electric field, space charge and orientation polarization have not and will induce frequency dispersion. A semi-quantitative analysis is followed to illustrate the contribution of the three kinds of polarizations.

The total polarization can be written as:

$$P = (n_e\alpha_e + n_s\alpha_s + n_o\alpha_o)E \quad (1)$$

Where n's mean the concentrations of lattice oxygen (which is related to electronic polarization), oxygen vacancies (which is related to trapped charges as part of space charge polarization) and oxygen coming from hydroxide (which is related to orientation polarization and mobile charge hopping as part of space charge polarization). α's mean polarizability, the subscripts e, s and o mean electron, space charge and orientation, respectively. All the polarizabilities are functions of the frequency.

Following our discussions, the electron polarizability α_e should be a constant. The other two polarizabilities have similar formulas like Debye's model:

$$\alpha = \alpha_0 + \frac{\alpha_1}{1 + i\omega\tau} \quad (2)$$

Where τ is relaxation time, α_0 is the optical polarizability and $\alpha_0 + \alpha_1$ is static polarizability. In our model we suppose they change little with the annealing temperature. Consider that the electron polarizability is almost independent with the frequency, after combining the coefficients, we have:

RSC Advances Accepted Manuscript

$$\alpha = n_e\alpha_e + n_s(\alpha_{0,s} + \frac{\alpha_{1,s}}{1+i\omega\tau_s}) + n_o(\alpha_{0,o} + \frac{\alpha_{1,o}}{1+i\omega\tau_o}) \quad (3)$$

Where the subscripts such as 0, 1 and e, s, o have the same meanings as above. Considering the capacitance density and the polarization have a linear relationship about the macro shape of the device, we use A and B to replace α_0 and α_1 because the difference between them is just a constant:

$$C = n_e A_e + n_s(A_s + \frac{B_s}{1+i\omega\tau_s}) + n_o(A_o + \frac{B_o}{1+i\omega\tau_o}) \quad (4)$$

At the low frequency range, the capacitance difference between 20Hz and 5000Hz of the five samples increases as temperature increases, but the percentage of hydroxyl group decreases, which indicates that the orientation polarization claims little responsibility on the frequency dispersion in low frequency range. Now, the total capacitance can be rewritten as:

$$C = n_e A_e + n_s(A_s + \frac{B_s}{1+i\omega\tau_s}) \quad (5)$$

The real part of (5) can correspond to our experiment results of the capacitance density. However, because space charge polarization relates to both oxygen vacancies and hydroxyl sites, here we divide the total space charge polarization into two parts. One part comes from the contribution of trapped charges and another comes from mobile charge hopping. The two are only differ by a constant of proportionality. Now, the real part of total capacitance density, which relates to the experimental capacitance - frequency results can be rewritten as:

$$\mathrm{Re}(C) = n_e A_e + n_{\text{s-vac}}(A_{\text{s-vac}} + \frac{B_{\text{s-vac}}}{1+\omega^2\tau_{\text{s-vac}}^2}) + n_{s\text{-OH}}(A_{s\text{-OH}} + \frac{B_{s\text{-OH}}}{1+\omega^2\tau_{s\text{-OH}}^2}) \quad (6)$$

This equation will be used to fit the experimental results which is obtained in vacuum to exclude proton conduction effect.

We can estimate A_e with the permittivity of pure Al_2O_3, supposing our device are full filled with Al_2O_3, we get A_e=197 nF/cm^2. As we know, the concentrations obtained from the XPS data is not strictly quantitative, here we select the data of anneal

RSC Advances Accepted Manuscript

temperatures of 240°C and 260°C to fit with formula (6). We let n_e, $n_{s\text{-vac}}$ and $n_{s\text{-OH}}$ are the same to the concentrations of lattice oxygen (Al-O-Al), oxygen vacancies (O_{vac}) and oxygen in hydroxide (-OH) separately. Comparison between the fitting and experiment results are shown in figure 10. The fitted data are listed in table 1. It suggests the relaxation time for space charge polarization is approximately to the order of 10^{-4} to 10^{-3}.

To further demonstrate dielectric polarization mechanism, temperature dependence of dielectric performances of the sample annealed under 240 °C were measured in vacuum. Capacitance-frequency dependency and Cole-Cole plot were shown in figures 11(a) and (b), respectively. With increasing the measuring temperature, the sample exhibits increased frequency dispersion in low frequency range. This phenomenon is attributed to an increased hopping probability of space charge, as a result of raised activation energy. By combining of capacitance performance which is close to the end of high frequency range (10 KHz to 1 MHz) and Cole-Cole plot, the corresponding Debye relaxation time can be obtained with:

$$\tau = 1/2\pi f \quad (7)$$

Where f is the frequency with maximum imaginary part on the arc, they are 700 KHz at 330 K and 630 KHz at 370 K. The Debye relaxation time are 2.3×10^{-7} s at 330 K and 2.5×10^{-7} s at 370 K. At 293K, the frequency with maximum imaginary part is beyond our measuring range (> 1 MHz). Higher measuring temperature leads to an increase of relaxation time. Therefore this relaxation in 10 KHz to 1 MHz range is related to orientation polarization, featured by the rotational process, which encounters a resistance due to thermal agitation.

Structural properties of IGZO thin films were also characterized by *x*-ray diffractometer, shown in figure 12. Due to the weak intensity of diffraction peaks, which were almost in the same order of background noise, the thin films are regarded as amorphous phase. Measurements of TFT transfer and output characteristics were also carried out. Device configuration and electrical characteristics were shown in figures 13(a), (b), (c), S(1)[35]. The field effect mobility (μ_{sat}) of the TFTs is extracted in the

RSC Advances Accepted Manuscript

saturation region of the transfer curve by the following equation:

$$I_{\mathrm{D,sat}} = \frac{w}{2L}\mu_{\mathrm{sat}} C_{\mathrm{ox}} (V_{\mathrm{G}} - V_{\mathrm{T}})^2 \qquad (8)$$

Where I_D is the drain to source current, V_G is the gate to source voltage, V_T is the threshold voltage, W and L are the channel width and length, respectively, and C_{ox} is the capacitance per unit area of the gate dielectric. By matching the transfer performance measurement, the capacitance at low frequency is often adopted to calculate mobility. Here the value at 100 Hz of Al_2O_3 dielectric capacitance-frequency characteristic was selected. Sub-threshold swing (SS) was calculated using the following equation:

$$SS = \mathrm{d}V_{\mathrm{G}} / \mathrm{d}(\log I_{\mathrm{D}}) \qquad (V_{\mathrm{G}} < V_{\mathrm{T}}) \qquad (9)$$

By utilizing SS value, the maximum interface trap states ($N_{\mathrm{trap}}^{\mathrm{max}}$) can also be calculated from the following equation:

$$N_{\mathrm{trap}}^{\mathrm{max}} = \left(\frac{qS\log e}{k_{\mathrm{B}}T} - 1\right) \cdot \frac{C_{\mathrm{ox}}}{q} \qquad (10)$$

Device parameters were summarized in table 2. By comparing device parameters comprehensively, sample obtained after annealing at 260 °C shows the best performances, with a mobility of 2.26 $cm^2V^{-1}s^{-1}$, a zero threshold voltage, a I_{on}/I_{off} of around 3×10^4, a sub-threshold swing of 186 mV/decade, and a maximum trap density of 4.2×10^{12} $cm^{-2}eV^{-1}$. However, sample obtained after annealing at 220 °C is also operable, albeit with an inferior mobility of 0.12 $cm^2V^{-1}s^{-1}$, a threshold voltage of only −1.27 V, a I_{on}/I_{off} of 2×10^3, a sub-threshold swing of 447 mV/decade, and a maximum trap density of 1.3×10^{13} $cm^{-2}eV^{-1}$. In regards to this type of semiconductors, for example, amorphous IGZO, their carrier transport results from direct overlap among the neighboring metal *ns* orbitals.[15] The magnitude of this overlap is insensitive to distorted metal-oxygen-metal (M-O-M) chemical bonds that intrinsically exist in amorphous materials.[14] Owing to both oxygen vacancy and traps, the TFT mobility varies with sample annealing temperature. A continuous mobility increase is observed, when the temperature increases from 220 °C to 300 °C, which is believed to be related to pre-

RSC Advances Accepted Manuscript

filling trap sites generated by oxygen vacancy, and/or distortional relaxation reduced trap sites.[36] Increasing annealing temperature higher than 260 °C, the mobility enhances slowly and approaches to its saturation. A negative threshold voltage indicates that the TFT operation mode is depletion one, in which the channel is activated as normally on. This implies that electrons are accumulated at the interface between dielectric and active layer, requiring a negative gate bias to deplete them. Besides the interface charges, the trap density also plays an important role in threshold voltage, Such as hydroxyl groups, which can be viewed as electron trap sites that attracting electrons and limiting its movement. Therefore, trap density affects free carriers number. A higher number meant it is easier to make carriers accumulate in the semiconductor/dielectric interface, hence contributes a small threshold voltage. In other words, a reduction of trap density always gives rise to a shift of threshold voltage toward a negative bias direction. It also means that a higher trap density requires a larger gate voltage to turn on the device. Relative phenomenon was found in other work as well. [37] In comparison with their electric hysteresis from dual drain voltage sweep, ΔV_T is less than –0.1 V, which can be ignored. The clockwise hysteresis effect, shown in figure 13(b), is due to IGZO/Al_2O_3 interface. Under a positive gate bias, it is possible that electrons are injected from IGZO into Al_2O_3 dielectrics, accompanied by a decrease in the carrier density in the vicinity of IGZO/Al_2O_3 interface, thus lowering I_D level and enhancing a more positive threshold voltage in the transfer reverse sweep.[9] Similar phenomenon was also found in sputtered Al_2O_3 dielectrics. I_{on}/I_{off} is determined by both off-current and on-current. A small off-current will be obtained, as long as the dielectric exhibits a low leakage current density, and the semiconducting active channel has a low concentration of oxygen vacancies. A large on-current will be obtained, if the device performs a high carrier mobility. Therefore, they contributes a good I_{on}/I_{off}. Devices sub-threshold swing are 447 mV/decade, 375 mV/decade, 186 mV/decade, 265 mV/decade, 372 mV/decade, for samples annealed at 220 °C, 240 °C, 260 °C, 280 °C and 300 °C, respectively. In general, the sub-threshold swing is an indicator of the total trap density including the bulk trap density of the semiconductor itself and the interface trap density in the vicinity

RSC Advances Accepted Manuscript

of the interface between semiconductor and dielectric layers.[38] The 260 °C annealed sample exhibits minimum sub-threshold swing, giving a relative fast response or switch speed. Concluded from our previous experiments, we find both dielectric and semiconductor layers account for the non-monotonic dependence. As a significant role, higher roughness of dielectric surface degrades TFTs performance due to scattering of electrons. Besides, when the solution processed semiconductor layer is under annealing, the thermal treatment also affects the dielectric layer. The reason might be the interdiffusion among Al^{3+}, In^{3+}, Ga^{3+} and Zn^{2+}, which has been also discussed in other's work.[39 40] In our experiment, it is suggested that In^{3+}, Ga^{3+} and Zn^{2+} in the combustion solution should be more likely to diffuse into Al_2O_3 layer at higher treatment temperature because of 1) they are more free to move in the solution than bonded Al^{3+} in Al_2O_3 layer, and 2) On account of the self-energy generated combustion process, those ions are easily activated to diffuse into Al_2O_3 layer and degrade device performance.

3. Experimental Procedures

Material synthesis

All chemicals were supplied by Sigma-Aldrich. Aluminum nitrate solution was prepared by dissolving 1.149 g aluminum nitrate nonahydrate ($Al(NO_3)_3 \cdot 9H_2O$, 99.997%) in 10 ml 2-methoxyethanol, which was vigorously stirred at 50 °C until a transparent solution formed. Then 0.4 ml acetylacetone and 0.2 ml $NH_3 \cdot H_2O$ were dropped in and the solution was followed by vigorously stirring overnight at 50 °C to achieve a homogeneous stable one. For the preparation of IGZO active layer, doping of indium was aimed to increase TFTs mobility due to the overlap of 5*s* orbitals of indium atoms, while doping of gallium was aimed at enhancing the semiconductor stability owing to a strong bond energy between gallium and oxygen atom. However, when the concentration of gallium was great than 20%, a degradation of mobility occurred.[26] Hence we selected the mole ratio of In: Ga: Zn of 65:10:25. IGZO solution was prepared by dissolving 0.075 g zinc nitrate hexahydrate ($Zn(NO_3)_2 \cdot 6H_2O$, 99.999%), 0.196 g

RSC Advances Accepted Manuscript

indium nitrate hydrate ($In(NO_3)_3 \cdot xH_2O$, 99.9%), 0.026 g gallium nitrate hydrate ($Ga(NO_3)_3 \cdot xH_2O$, 99.9%) in 10 ml 2-methoxyethanol, which was vigorously stirred at 50 ºC until all nitrates dissolved. Afterwards 0.2 ml acetylacetone and 0.1 ml $NH_3 \cdot H_2O$ were dropped in, and the solution was vigorously stirred overnight at 50 ºC to form a homogeneous stable one.

Thin film fabrication

P^{++}–Si substrates were sonicated with acetone and ethanol, followed by nitrogen gas purging. Afterwards a 5 min oxygen plasma treatment was conducted to clean the surface. Before spin coating, both solution were filtered through a 0.22 μm PTFE membrane syringe filters. P^{++}–Si substrates were heated at 120 ºC for 10 min on a hot plate before spin coating. Then aluminum nitrate solution was spin-coated at 3000 rpm for 10 s. After spin coating, the substrates were placed on a hot plate and annealed at 120 ºC for 10 min, then annealed at 160 ºC for 10 min, followed by annealing at 220 ºC for 30 min, finally annealed at intended IGZO treatment temperature for 1 h. The reason for step annealing was due to high-reactivity of aluminum ion. If a combustion process for aluminum oxide layer was categorically conducted, which meant the spin-coated films were heated directly at 220 ºC, on account of sharp combustion reaction, poor quality films would be formed with a mass of pores, leading to a high leakage current. Relevant phenomenon was also reported in other works.[41] However, if the films were heated at a low temperature firstly, the input energy was insufficient to initiate the combustion process, meanwhile the fuel - acetylacetone, would also volatilized. Thus compared to the combustion process, the oxidation reaction slowed down to avert gas pore formation. Therefore, in this dielectric film fabrication process, the acetylacetone was conducive to a definitely successful spin-coating process to attain the hydrophilicity of solution matching greatly with highly doped silicon, but did not serve as a fuel. Thus the process is just a conventional oxidizing process instead of combustion, in which the additive plays a role to improve solution wettability, albeit the same recipe as IGZO solution. To guarantee a high breakdown voltage and low

RSC Advances Accepted Manuscript

leakage current, another spin-coating process was repeated. After the substrate coated with the aluminum oxide layer, spin-coating time could be extended to 20 s. The 2-layer dielectrics had a thickness of ~ 45 nm. Before IGZO thin film spin-coated, aluminum oxide was pre-heated at 120 ^{o}C for 10 min. The solution was spin-coated on it at 3000 rpm for 10 s, then annealed directly at intended temperature (220 ^{o}C ~ 300 ^{o}C) for 1 h to proceed to the combustion reaction. Also the procedure was repeated once but spin-coating time extended to 20 s. The 2-layer active channel was achieved with a thickness of ~ 30 nm.

Device fabrication

To characterize electrical properties of gate dielectric, a 100 nm-thick circular Al top electrode was deposited onto aluminum oxide film by thermal evaporation process via a shadow mask (electrode radius was 100 μm) to construct a metal-insulator-metal (MIM) structure. To fabricate TFTs, a bottom gate, top contact structure was used because its easy handling. Also a 100 nm-thick Al source and drain electrodes were deposited on IGZO thin film by thermal evaporation through a shadow mask. The width of channel (W) was 1500 μm, and length of channel (L) was 50 μm. 9 devices of each temperature were fabricated and the average performances were given.

Characterization methods

The contact angles of solutions was measured with a contact angle microscope. *x*-ray diffraction analysis of gate dielectrics and active channel was performed by Siemens D5005 *x*-ray diffractometer using Cu K_{α} radiation. Surface morphologies of Al_2O_3 and IGZO thin film were characterized by atomic force microscope (AFM), Vecco Nanoscope IIIa. *x*-ray photoelectron spectroscopy was carried out by VG Scientific ESCALAB 250. The frequency-dependent capacitance of MIM structure was measured by HP 4284A, in a frequency range from 20 Hz to 1 MHz. Breakdown voltage and leakage current of MIM structure were measured by Keithley 4200 SCS Analyzer under ambient conditions. TFTs characteristics were also characterized by Keithley 4200 SCS

RSC Advances Accepted Manuscript

Analyzer under ambient conditions.

4. Conclusions

In this report, all solution-processed IGZO thin film transistors (TFTs) with Al_2O_3 gate dielectrics were successfully fabricated at low temperature and low cost. Using acetylacetone and aqueous ammonia as an additive, aluminum nitrate solution can be spin-coated on highly doped silicon easily and forms a fully covered continuous film. Good quality amorphous Al_2O_3 gate dielectrics were obtained with a solution process at a low temperature of 220 °C. By utilizing combustion process for IGZO thin film fabricated on the top of Al_2O_3 gate dielectric, a high quality TFTs has been fabricated at a low temperature of 240 °C. Combination of combustion-processed active layers and solution-processed high-k dielectrics provides a feasible approach for low-cost flexible oxide TFTs applications, such as utilizing polyimide substrate after selecting a proper gate electrode.

5. Acknowledgements

The work is in part supported by Research Grants Council of Hong Kong, particularly, via Grant Nos. AoE/P-03/08, N_CUHK405/12, and CUHK Group Research Scheme. J. B. Xu would like to thank the National Science Foundation of China for the support, particularly, via Grant No 61229401.

Figures and Figure Captions

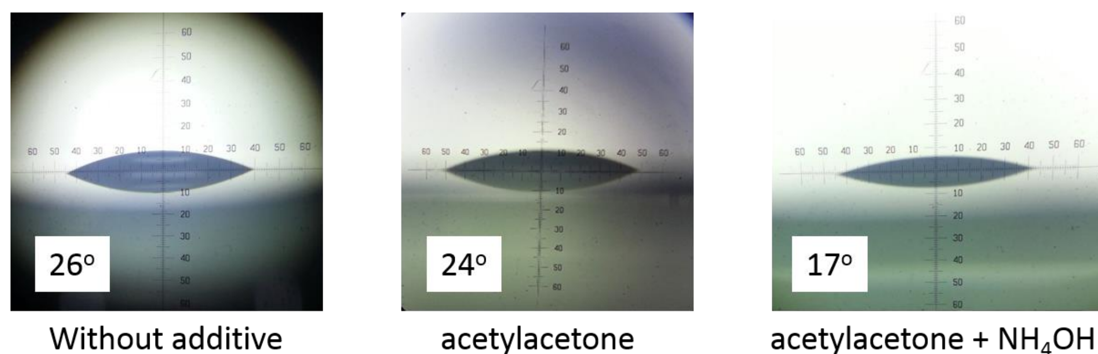

RSC Advances Accepted Manuscript

Figure 1. Contact angle measurements of solution without additive, with acetylacetone only and with acetylacetone plus aqueous ammonia. The substrates are highly doped silicon without oxygen plasma treatment.

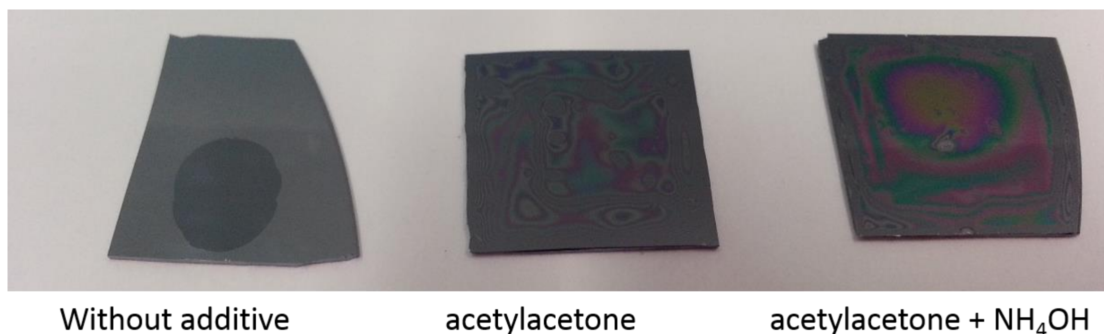

Figure 2. Wettability comparison of conventional solution, conventional solution with acetylacetone only and our novel solution. The substrates are oxygen plasma treated highly doped silicon.

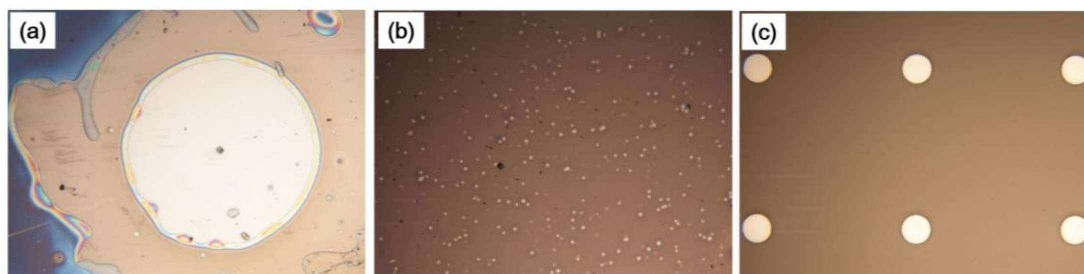

Figure 3. Optical microscope pictures of the samples, all of which are 2 layers, all of the annealed temperatures are 220 ℃, and all of the magnifications are ×50. (a) Using conventional solution without additive. (b) Using novel solution to conduct a combustion reaction, annealing at 220ºC directly. (c) Using novel solution and conducting step annealing, starting temperature is 120ºC (to avoid combustion reaction).

RSC Advances Accepted Manuscript

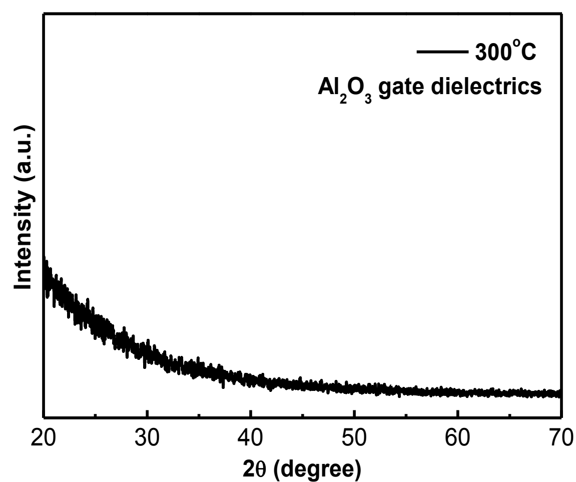

Figure 4. *x*-ray diffraction characterization of Al_2O_3 gate dielectric thin film annealed at 300 °C.

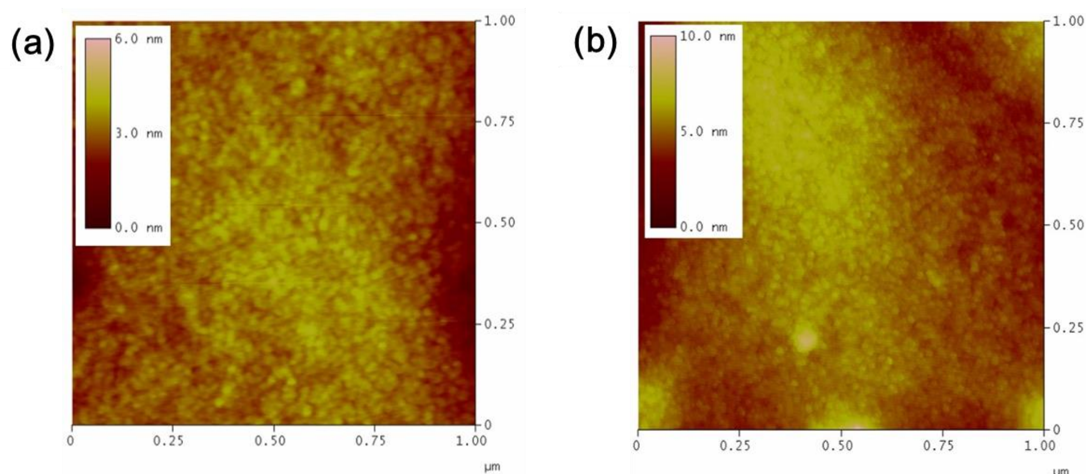

Figure 5. (a) AFM characterization of Al_2O_3 gate dielectric thin film surface annealed at 220 °C. RMS is about 0.5 nm. (b) AFM characterization of Al_2O_3 gate dielectric thin film surface annealed at 300 °C. RMS is about 1.1 nm.

RSC Advances Accepted Manuscript

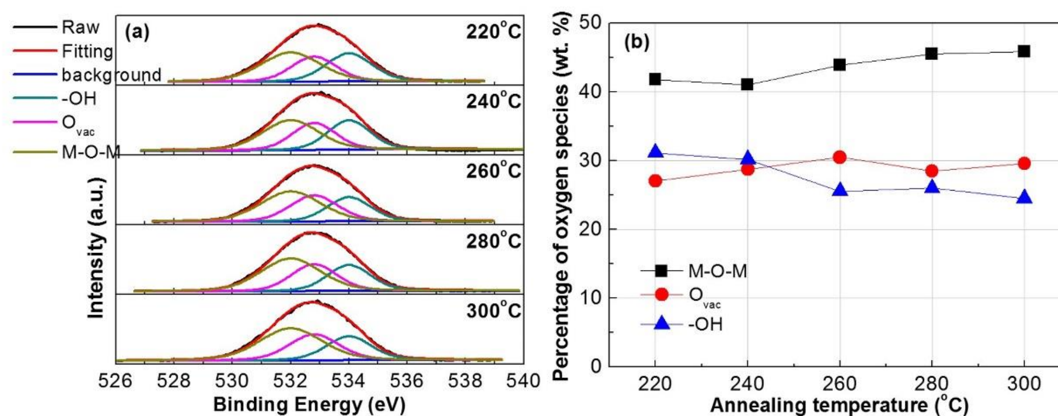

Figure 6. (a) O_{1s} XPS spectra of Al_2O_3 gate dielectric thin films annealed at 220 ºC, 240ºC, 260ºC, 280ºC and 300 ºC. (b) Dependency of percentage of oxygen species and annealing temperature.

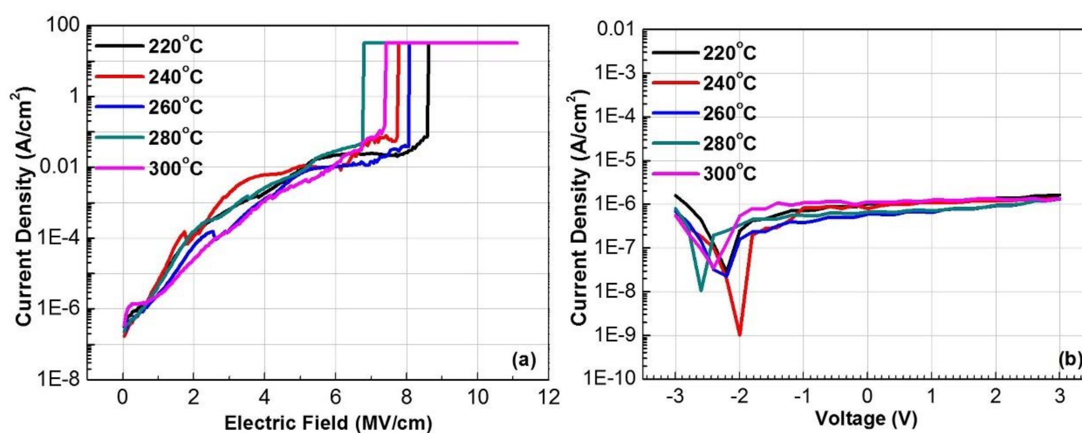

Figure 7. (a) Current density versus electric field characteristics of MIM structure of Al_2O_3 gate dielectric thin films annealed from 220 ºC to 300 ºC. (b) Current density versus applied voltage characteristics of MIM structure of Al_2O_3 gate dielectric thin films annealed from 220 ºC to 300 ºC.

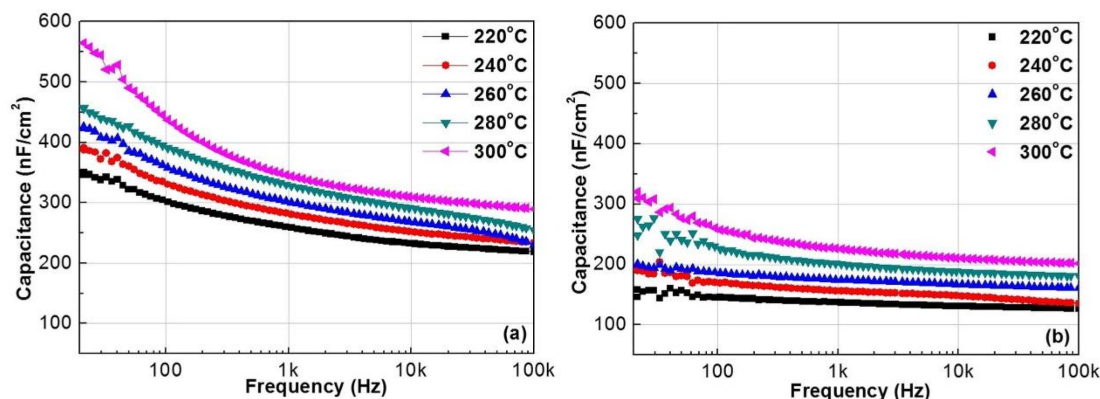

RSC Advances Accepted Manuscript

Figure 8. (a) Dielectric capacitance versus frequency of Al_2O_3 gate dielectric thin films annealed from 220 ºC to 300 ºC, characterized in ambience, voltage bias was 3 V. (b) Dielectric capacitance versus frequency of Al_2O_3 gate dielectric thin films annealed from 220 ºC to 300 ºC, characterized in vacuum, voltage bias was 3 V.

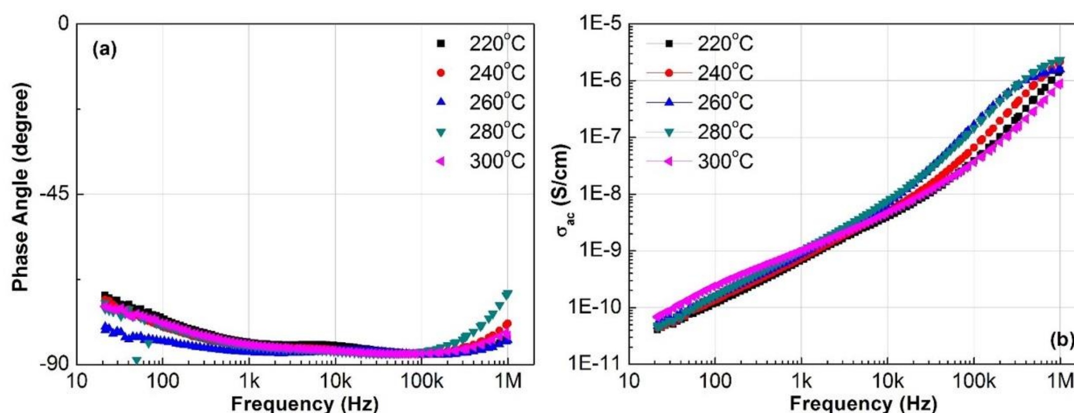

Figure 9. (a) Phase angle versus frequency of Al_2O_3 gate dielectric thin films annealed from 220 ºC to 300 ºC, characterized in ambience, voltage bias was 3 V. (b) Conductivity versus frequency of Al_2O_3 gate dielectric thin films annealed from 220 ºC to 300 ºC, characterized in ambience, voltage bias was 3 V.

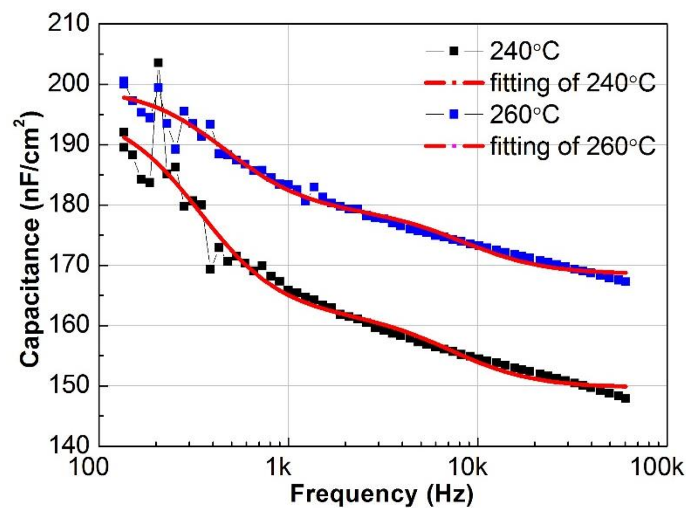

Figure 10. Least Square fitting of capacitance - frequency dependency.

RSC Advances Accepted Manuscript

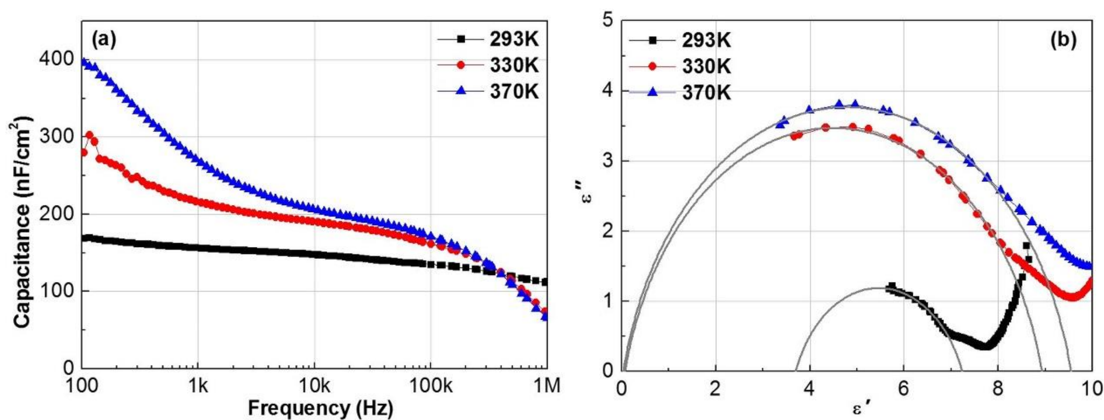

Figure 11. (a) Capacitance-frequency dependency of sample annealed at 240 °C via varying of measuring temperature from 293 K to 370 K in vacuum. (b) Cole-Cole plot (*ε''* vs *ε'*) of sample annealed at 240 °C, measured in vacuum.

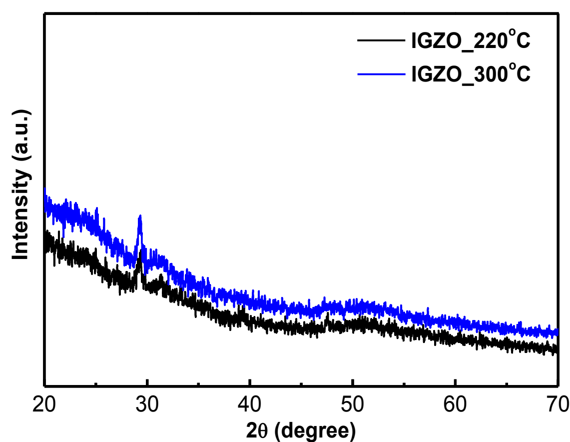

Figure 12. *x*-ray diffraction characterization of IGZO active layer annealed at 220 °C and 300 °C.

RSC Advances Accepted Manuscript

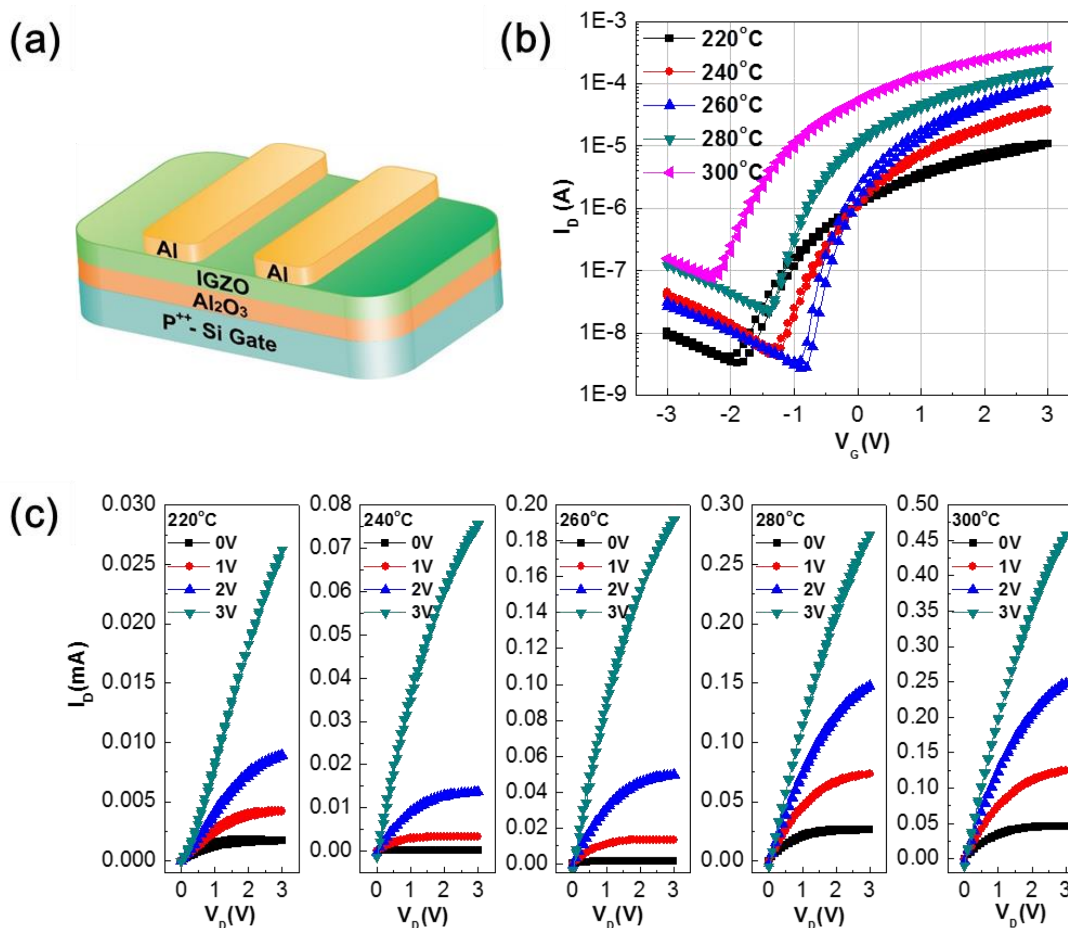

Figure 13. Device configuration and electrical characteristics of TFTs composed of combustion-processed IGZO active channel with spin-coated Al_2O_3 gate dielectrics. (a) device configuration; (b) transfer and (c) output characteristics of IGZO TFTs annealed from 220 ºC to 300 ºC.

Table 1. Least Square fitting data of capacitance - frequency dependency characterized in vacuum.

Capacitance – frequency dependency fitting results						
T (ºC)	$A_{s\text{-vac}}$ (nF/cm^2)	$B_{s\text{-vac}}$ (nF/cm^2)	$\tau_{s\text{-vac}}$ (s)	$A_{s\text{-OH}}$ (nF/cm^2)	$B_{s\text{-OH}}$ (nF/cm^2)	$\tau_{s\text{-OH}}$ (s)
240	239	41	0.0001	0.7	113	0.0029
260	267	34	0.0001	0.3	80	0.0022

Table 2. Electrical parameters of combustion processed IGZO TFTs fabricated using

RSC Advances Accepted Manuscript

Al_2O_3 gate dielectric films annealed from 220 °C to 300 °C.

TFTs Electrical Performances						
T (°C)	C_{ox} (nF/cm^2)	μ (cm^{2}V^{-1}s^{-1})	V_T (V)	I_{on}/I_{off}	SS (mV/decade)	N_{trap}^{max} (cm^{-2}eV^{-1})
220	317	0.12	−1.3	2×10^3	447	1.3×10^{13}
240	291	0.74	−0.4	6×10^3	375	9.6×10^{12}
260	319	2.26	0	3×10^4	186	4.2×10^{12}
280	405	2.28	−0.5	7×10^3	265	8.7×10^{12}
300	377	2.82	−1.9	4×10^3	372	1.2×10^{13}

References:

1. S. Masuda, K. Kitamura, Y. Okumura, S. Miyatake, H. Tabata and T. Kawai, Journal of Applied Physics **93** (3), 1624 (2003).
2. J.-S. Park, H. Kim and I.-D. Kim, Journal of Electroceramics (2013).
3. H. Q. Chiang, J. F. Wager, R. L. Hoffman, J. Jeong and D. A. Keszler, Applied Physics Letters **86** (1), 013503 (2005).
4. V. Subramanian, T. Bakhishev, D. Redinger and S. K. Volkman, J. Display Technol. **5** (12), 525-530 (2009).
5. R. John, Reports on Progress in Physics **69** (2), 327 (2006).
6. Y. Su, C. Wang, W. Xie, F. Xie, J. Chen, N. Zhao and J. Xu, ACS applied materials & interfaces **3** (12), 4662-4667 (2011).
7. K. Song, W. Yang, Y. Jung, S. Jeong and J. Moon, Journal of Materials Chemistry **22** (39), 21265 (2012).
8. P. K. Nayak, M. N. Hedhili, D. Cha and H. N. Alshareef, Applied Physics Letters **103** (3), 033518 (2013).
9. M. S. Oh, K. Lee, J. H. Song, B. H. Lee, M. M. Sung, D. K. Hwang and S. Im, Journal of The Electrochemical Society **155** (12), H1009 (2008).
10. Y. B. Yoo, J. H. Park, K. H. Lee, H. W. Lee, K. M. Song, S. J. Lee and H. K. Baik, Journal of Materials Chemistry C **1** (8), 1651 (2013).

RSC Advances Accepted Manuscript

11. A. H. Chen, L. Y. Liang, H. Z. Zhang, Z. M. Liu, X. J. Ye, Z. Yu and H. T. Cao, Electrochemical and Solid-State Letters **14** (2), H88 (2011).
12. S. Jeong, Y. G. Ha, J. Moon, A. Facchetti and T. J. Marks, Adv Mater **22** (12), 1346-1350 (2010).
13. T. Phan Trong, T. Miyasako, L. Jinwang, T. Huynh Thi Cam, S. Inoue, E. Tokumitsu and T. Shimoda, Electron Devices, IEEE Transactions on **60** (1), 320-326 (2013).
14. K. Nomura, H. Ohta, A. Takagi, T. Kamiya, M. Hirano and H. Hosono, Nature **432** (7016), 488-492 (2004).
15. K. H. Lee, J. H. Park, Y. B. Yoo, W. S. Jang, J. Y. Oh, S. S. Chae, K. J. Moon, J. M. Myoung and H. K. Baik, ACS applied materials & interfaces **5** (7), 2585-2592 (2013).
16. S. Jeong, J.-Y. Lee, M.-H. Ham, K. Song, J. Moon, Y.-H. Seo, B.-H. Ryu and Y. Choi, Superlattices and Microstructures **59**, 21-28 (2013).
17. J. Li, L. Niu, Z. Zheng and F. Yan, Adv Mater (2014).
18. F. Yan, M. Zhang and J. Li, Advanced healthcare materials **3** (3), 313-331 (2014).
19. H. Bong, W. H. Lee, D. Y. Lee, B. J. Kim, J. H. Cho and K. Cho, Applied Physics Letters **96** (19), 192115 (2010).
20. Y. Zhao, G. Dong, L. Duan, J. Qiao, D. Zhang, L. Wang and Y. Qiu, RSC Advances **2** (12), 5307 (2012).
21. W. Xu, H. Wang, L. Ye and J. Xu, Journal of Materials Chemistry C (2014).
22. W. Xu, D. Liu, H. Wang, L. Ye, Q. Miao and J.-B. Xu, Applied Physics Letters **104** (17), 173504 (2014).
23. M.-G. Kim, H. S. Kim, Y.-G. Ha, J. He, M. G. Kanatzidis, A. Facchetti and T. J. Marks, J Am Chem Soc **132** (30), 10352-10364 (2010).
24. Y. H. Kim, J. S. Heo, T. H. Kim, S. Park, M. H. Yoon, J. Kim, M. S. Oh, G. R. Yi, Y. Y. Noh and S. K. Park, Nature **489** (7414), 128-132 (2012).
25. J. W. Hennek, M. G. Kim, M. G. Kanatzidis, A. Facchetti and T. J. Marks, J Am Chem Soc **134** (23), 9593-9596 (2012).
26. J. W. Hennek, J. Smith, A. Yan, M. G. Kim, W. Zhao, V. P. Dravid, A. Facchetti and T. J. Marks, J Am Chem Soc **135** (29), 10729-10741 (2013).

RSC Advances Accepted Manuscript

27. M. Lorenz, H. von Wenckstern and M. Grundmann, Adv Mater **23** (45), 5383-5386 (2011).

28. K.-C. Liu, J.-R. Tsai, W.-K. Lin, C.-S. Li and J.-N. Chen, Thin Solid Films **519** (15), 5110-5113 (2011).

29. H. Birey, Journal of Applied Physics **49** (5), 2898 (1978).

30. L. Herlogsson, X. Crispin, N. D. Robinson, M. Sandberg, O. J. Hagel, G. Gustafsson and M. Berggren, Advanced Materials **19** (1), 97-101 (2007).

31. G. Wu, H. Zhang, J. Zhou, A. Huang and Q. Wan, Journal of Materials Chemistry C **1** (36), 5669-5674 (2013).

32. H. Zhang, L. Guo and Q. Wan, Journal of Materials Chemistry C **1** (15), 2781-2786 (2013).

33. J. H. Park, K. Kim, Y. B. Yoo, S. Y. Park, K.-H. Lim, K. H. Lee, H. K. Baik and Y. S. Kim, Journal of Materials Chemistry C **1** (43), 7166-7174 (2013).

34. Y. Liu, P. Guan, B. Zhang, M. L. Falk and H. E. Katz, Chemistry of Materials **25** (19), 3788-3796 (2013).

35. See supplemental material at _______________for transfer performances including leakage.

36. M.-G. Kim, Kanatzidis, Mercouri G., Facchetti, Antonio, Marks, Tobin J., Nat Mater **10** (5), 7 (2011).

37. P. Barquinha, A. Pimentel, A. Marques, L. Pereira, R. Martins and E. Fortunato, Journal of Non-Crystalline Solids **352** (9–20), 1749-1752 (2006).

38. J. H. Jeong, H. W. Yang, J.-S. Park, J. K. Jeong, Y.-G. Mo, H. D. Kim, J. Song and C. S. Hwang, Electrochemical and Solid-State Letters **11** (6), H157 (2008).

39. X. Zou, G. Fang, L. Yuan, X. Tong and X. Zhao, Microelectronics Reliability **50** (7), 954-958 (2010).

40. S. Masuda, K. Kitamura, Y. Okumura, S. Miyatake, H. Tabata and T. Kawai, Journal of Applied Physics **93** (3), 1624-1630 (2003).

41. S. Y. Cho, E. J. Bae, Y. H. Kang, M. Han and C. Lee, Journal of Materials Chemistry C (2014).

RSC Advances Accepted Manuscript

RSC Advances Accepted Manuscript

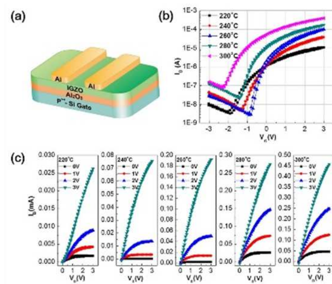

An improved hydrophilic aluminum nitrate solution was designed to spin coat robust dielectric layers for thin film transistors.

RSC Advances Accepted Manuscript